First ionospheric images of the seismic fault slip on the example of the Tohoku-oki earthquake

Elvira Astafyeva, Philippe Lognonné, Lucie Rolland

First ionospheric images of the seismic fault slip on the example of the Tohoku-oki earthquake

Elvira Astafyeva,[1,2] Philippe Lognonné,[1] and Lucie Rolland[1,3]

Received 13 September 2011; revised 25 October 2011; accepted 25 October 2011; published 24 November 2011.

[1] 1Hz GPS measurements from the Japanese GPS network GEONET allowed to retrieve information on the seismic fault of the great M9.0 Tohoku-oki earthquake from the ionosphere total electron content (TEC) measurements. The first arrival of the TEC perturbation was registered 464 seconds after the earthquake ~140 km on the east from the epicenter. Within next 45 seconds the distribution of ionospheric points imaged a rectangular area (37.39 - 39.28°N; 142.8 – 143.73°E), which coincides with the area of the coseismic crustal uplift. From this source region, the coseismic ionospheric perturbation further propagated at 1.3-1.5 km/s. Such velocity values are 30-40% higher than previously reported for acoustic waves. It is likely that we observed shock-acoustic waves propagating at supersonic speed and having blown all the electrons available between the ground and the height of detection. This fact is coherent with registration of the first arrival of perturbation 464 sec after the earthquake that is, generally speaking, too short time for a regular acoustic wave to reach the ionosphere. Our findings show that the real-time GPS monitoring of seismo-active areas could inform about the parameters of coseismic crustal displacements and can be, subsequently, used for short-term tsunami warnings. In the case of the 03/11/2011 earthquake, the first ionosphere perturbations were registered ~17 minutes before the tsunami arrived on the east coast of Honshu. **Citation:** Astafyeva, E., P. Lognonné, and L. Rolland (2011), First ionospheric images of the seismic fault slip on the example of the Tohoku-oki earthquake, *Geophys. Res. Lett.*, *38*, L22104, doi:10.1029/2011GL049623.

1. Introduction

[2] Surface vertical displacements from earthquakes are known to produce infrasonic atmospheric pressure waves that propagate upward and grow in amplitude by several orders of magnitude as they reach the ionosphere altitudes. Further, due to the coupling between neutral particles, ions and electrons in the ionosphere, these acoustic and gravity waves induce variations in the ionosphere electron density and its integrated quantity – total electron content (TEC) measurable using GPS [*Calais and Minster*, 1995; *Afraimovich et al.*, 2001; *Heki and Ping*, 2005; *Astafyeva and Afraimovich*, 2006; *Lognonné et al.*, 2006; *Astafyeva et al.*, 2009; *Rolland et al.*, 2011a].

[3] Co-seismic ionosphere disturbances (CID) are detectable in the vicinity of earthquake's epicenter and away from it. The perturbations can be generated by acoustic or shock-acoustic waves due to the co-seismic vertical crustal movement itself and by surface Rayleigh or tsunamis wave fronts. Depending on their source, CID differ in their features such as the waveform, propagation velocity, duration and period [*Astafyeva et al.*, 2009; *Rolland et al.*, 2011b].

[4] Strong ionospheric signals have been already reported following the Tohoku-oki earthquake, either close to the epicenter [e.g., *Rolland et al.*, 2011b, *Liu et al.*, 2011] or at large epicentral distance [*Makela et al.*, 2011]. Here we focus on the analysis of arrival times and amplitudes of the near-field co-seismic perturbations of TEC and on their correlation with the source structure. Such attempt was in the past only undertaken by *Heki et al.* [2006], who used ionosphere TEC measurements of GPS receivers to constrain the rupture process of the great Sumatra-Andaman earthquake. Although only nine GPS receivers were available for the Sumatra earthquake, the CID structure was found in accordance with the overall rupture process.

[5] We can therefore expect that 1Hz data of the world's densest GPS network GEONET (Japan) will reveal much higher resolution picture of the seismic source, and the aim of this paper is to provide the first of these ionospheric images for the seismic slip, with the further goal to extract parameters and location of the crustal movements associated with the Tohoku-oki earthquake from the ionosphere TEC observations.

2. M9.0 Tohoku-Chiho Taiheiyo-Oki Megathrust Earthquake

[6] A magnitude 9.0 earthquake occurred at 05:46:26 UT on 11 March 2011 off the east coast of Honshu, Japan, as a result of thrust faulting on or near the subduction zone interface plate boundary between the Pacific and North American plates. According to the US Geological Survey (The National Earthquake Information Center; http://earthquake.usgs.gov), the epicenter of this shallow earthquake is estimated at 32 km depth and located at 38.322°N and 142.369°E. Five minutes in duration, the earthquake generated a tsunami on the Pacific coast from the Hokkaido, Tohoku and Kanto regions, with tsunami maximum heights over 28 m around the Tohoku region of Japan.

[7] The location, depth, and focal mechanism of the March 11 earthquake are consistent with the event having occurred on the subduction zone plate boundary. Modeling of the rupture of this earthquake indicate that the fault moved upwards of 30–40 m, and slipped over an area approximately

[1]Institut de Physique du Globe de Paris, Paris Sorbonne Cité, Université Paris Diderot, UMR 7154, CNRS, Saint Maur des Fossés, France.
[2]On leave from Institute of Solar-Terrestrial Physics SB RAS, 126a Lermontova street, Irkutsk, Russia.
[3]Now at Géoazur/Nice University/Observatoire de la Côte d'Azur, UMR 6526, 250 rue Albert Einstein, Valbonne, France.

0094-8276/11/2011GL049623

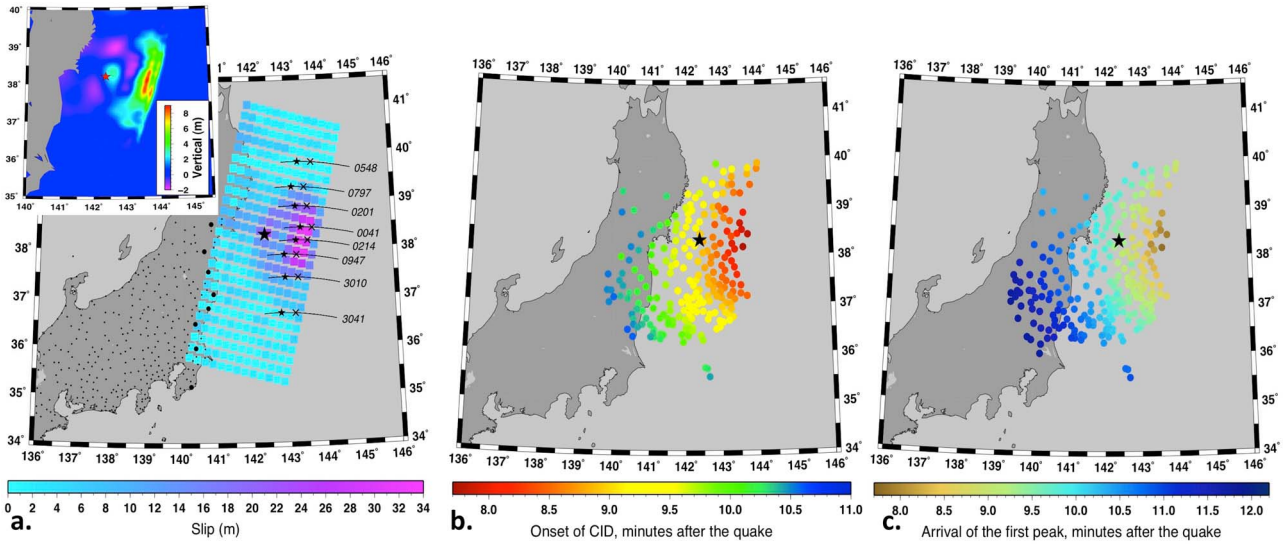

Figure 1. (a) General Information on the Tohoku-oki earthquake of 11 March 2011. Big black star represents the epicenter, squares indicate the location and length of the rupture zone. The color of the squares shows the slip amplitude (from http://earthquake.usgs.gov). Small black dots are the GEONET GPS receivers whose data we used in our work. Larger black dots represent some of GPS receivers whose SIP were located along the fault. Black curves show trajectories of SIP for the chain of receivers and PRN26, small black stars indicate positions of SIP at the time of the quake, black crosses – positions of the CID first arrivals (onsets). Panel in the left upper corner shows co-seismic vertical seafloor displacements calculated according to *Okada* [1992] using the coseismic slip distribution calculated by the USGS. (b–c) Spatial distribution of the ionospheric points corresponding to the first arrivals (Figure 1b) and first maximums (Figure 1c) of the co-seismic TEC perturbations detected by GPS satellite 26 at altitude 250 km. The color indicates the arrival time in minutes after the main quake at 05:46:23 UT. Black star shows the epicenter.

300 km long (along-strike) by 150 km wide (in the down-dip direction). The rupture zone is roughly centered on the earthquake epicenter along-strike, while peak slips were up-dip of the hypocenter, towards the Japan Trench axis (http://earthquake.usgs.gov and Figure 1a). The rupture was bilateral, i.e., it spread away from the epicenter in both the north and south directions, taking about 2 minutes to cover a total of 400 km [e.g., *Simons et al.*, 2011].

3. Co-Seismic TEC Perturbations and Seismic Rupture as Seen in the Ionosphere TEC

[8] Due to the dispersive nature of the ionosphere, dual frequency (1.2 and 1.5 GHz) GPS measurements can provide integral information about the ionosphere by computing the differential phases of code and carrier phase measurements recorded by ground-based GPS receivers. Methods of TEC calculation have been described in detail in a number of papers [e.g., *Calais and Minster*, 1995; *Afraimovich et al.*, 2001]. To eliminate variations of the regular ionosphere, as well as trends introduced by the orbital motion of a satellite, we firstly smoothed the initial 1 Hz TEC series with time window of 3 sec (by running mean) and then removed the linear trend with a window of 20 min. This works as a band-pass filter to extract variations with period 3 sec–20 min, which is suitable for studying fast ionosphere disturbances.

[9] Since TEC is an integral parameter, it is impossible to determine the height of ionospheric disturbance using measurements from one satellite. However, the main contribution to TEC variations appears around the height of the ionosphere maximum ionization. This allows us to consider the ionosphere as a thin layer located at the h_{max} height of the ionosphere F2 layer. TEC then represents a point of intersection of a line-of-sight with this thin layer. We trace propagation of CID by subionospheric point (SIP), a projection of an ionospheric piercing point to the earth's surface. In this paper we assumed h_{max} as 250 km.

[10] Low elevation angles tend to enlarge the horizontal extent of the ionospheric region represented by one measurement. During the earthquake the elevation angles varied from 35 to 41 degrees that is low enough to enlarge the sphericity effects. Therefore, we converted the slant TEC to vertical TEC by using the known Klobuchar's formula [*Klobuchar*, 1986].

[11] During the earthquake, ten GPS satellites passed around and over the Japanese islands. However, only TEC measurements of satellite PRN 26 were useful for our study of co-seismic TEC perturbations above the focal regions of the quake and of CID forming. As seen from Figure 1a, the satellite sounding points passed over the epicenter and the seismic fault that ruptured during the earthquake. TEC variations recorded in the vicinity of the seismic fault are shown in Figure 2a.

[12] Despite some GPS stations were only ~20-30 km distant from one another, the amplitude and the shape of the variations differed. The maximum amplitude was registered at the southernmost receivers (3009, 3010), while the minimum corresponds to the northernmost receivers (0559, 0797) (Figure 2a and Figure S1 from the auxiliary material)[1]. Such distribution can be caused by the influence of geomagnetic field and by the geometry of GPS sounding. It is

[1]Auxiliary materials are available in the HTML. doi:10.1029/2011GL049623.

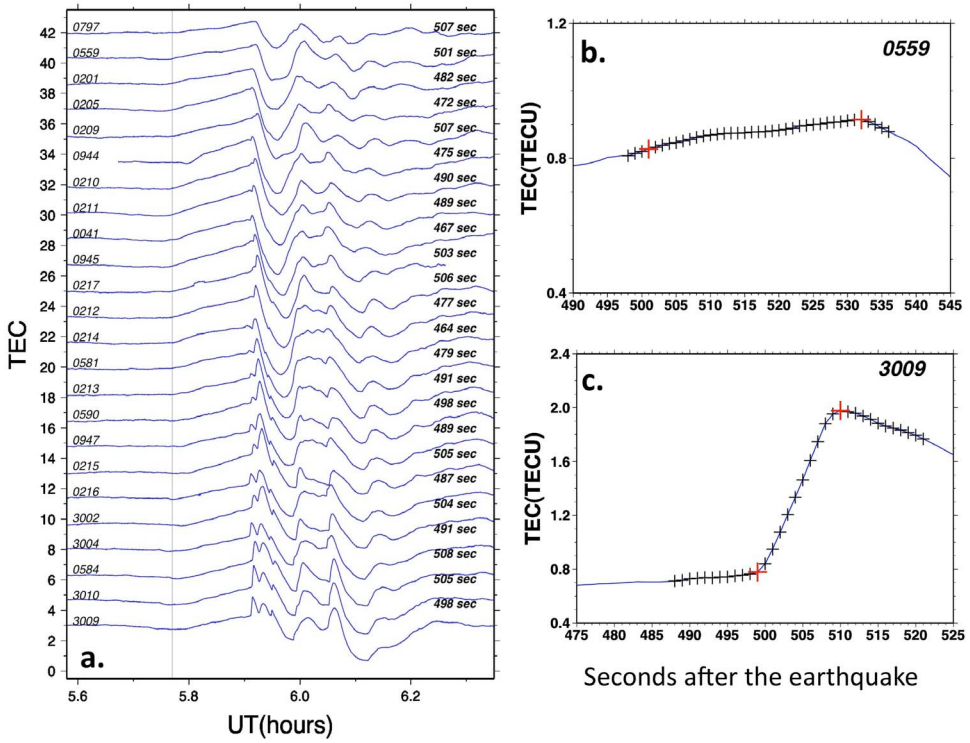

Figure 2. (a) Co-seismic TEC variations recorded by satellite PRN26. TEC is shown in relative TECU. The time of the earthquake 05:46:23 UT is shown by thin vertical line. Names of GPS receivers are indicated on the left side, and on the right side the perturbation arrival time is shown in seconds after the earthquake. (b–c) TEC time-series recorded by GPS receivers 0559 (Figure 2b) and 3009 (Figure 2c) during 50–55 sec. Black crosses demonstrate the advantages of the high-rate 1sec sampling, red crosses indicate positions of the onset and of the first maximum of TEC perturbation.

known that in northern hemisphere at mid-latitudes geomagnetic field impedes northward propagation and favours the southward propagation of ionospheric disturbances [e.g., *Calais and Minster*, 1995; *Afraimovich et al.*, 2001; *Kherani et al.*, 2009; *Rolland*, 2011a]. However, *Astafyeva and Heki* [2009] showed that northward propagated TEC perturbations are detectable within 100 km from the source before they fade out. Besides, the positive phase of the initial N-wave of a northward propagating disturbance diminishes much faster than that of negative phase [*Astafyeva and Heki*, 2009]. From these facts and from the latitudinal distribution of GPS receivers in Figure 2a we can estimate that the approximate position of the CID source was elongated from ~38.5°N (site 0944) to ~37.6°N (site 3004). Figure S1 limits the position of the CID source (37.7-39°N; 143–143.8°E), since from this region the amplitude of CID increases with southward propagation and decreases with northward propagation.

[13] Figure 2a clearly shows that the observed co-seismic TEC variations are superimposed signals, which makes it difficult to analyze the dynamic characteristics of the CID. The arrivals of the disturbance were first estimated from the time and the coordinates of the SIP of the first arrival of the perturbation, i.e. the moment when TEC rapidly increases. As another "benchmark", we further determined the time and the coordinates of the first maximums of the TEC data series. For the northernmost located GPS stations that do not show clear TEC peaks, we considered the maximum before the rapid TEC decrease, to be the first maximum. At the same time, it was rather difficult to estimate the onset of the perturbations recorded at the northernmost stations (such as 0559 and 0797 in Figures 2a and 2c). In this case, more detailed analysis of the TEC variations allowed defining approximately the arrival time, even if with an error exceeding few seconds, though that 1 Hz data allow determining of these parameters with unprecedented accuracy (Figures 2b and 2c). Note also that our filtering method does not shift the time of TEC variations peaks. Positions of the SIP corresponding to the CID onset time and their first maximums are shown in Figures 1b and 1c, respectively.

[14] The very first arrival of perturbation was registered at station 0214 at 05:54:07 Universal Time (UT), i.e. 464 sec after earthquake time (05:46:23 UT) at point with coordinates 38.18°N; 143.59°E (Figure 1b and Table 1). Three and eight seconds later respectively, the second and third arrivals were recorded at point 38.44°N; 143.73°E (station 0041) and point 38.67°N; 143.51°E (station 0205). Thus, within first 15 seconds the SIP imaged a region (38.13 - 38.66°N; 143.28 – 143.72°E), during next 15 seconds the CID propagated mostly northward and southward simultaneously, so that by 05:54:51 UT (45 seconds after the first arrival) the CID imaged area (37.42–39.28°N; 142.80–143.72°E). From this "original" area CID propagates further away in all directions though PRN26 mostly allowed to detect westward and north- and south-westward propagation of CID. Unfortunately, the geometry of GPS receivers does not allow observations within ~0.6° of latitude on the south from the first arrival point. However, from the subsequent isotropic propagation of CID we could presume the arrivals of

Table 1. Parameters of the Onsets of TEC Perturbations[a]

GPS Site	Arrival Time (hh:mm:ss)	Sec After the Quake	Lon (°E), Lat (°N) of SIP
0214	05:54:07	464	143.586 38.178
0041	05:54:10	467	143.726 38.442
0205	05:54:15	472	143.506 38.668
0944	05:54:18	475	143.557 38.533
0212	05:54:20	477	143.280 38.248
0581	05:54:22	479	143.356 38.134
0201	05:54:25	482	143.602 38.883
0216	05:54:30	487	143.344 37.765
0947	05:54:32	489	143.262 37.890
0211	05:54:32	489	143.425 38.452
0210	05:54:33	490	143.147 38.499
0213	05:54:34	491	143.177 38.055
3004	05:54:34	491	143.409 37.610
0590	05:54:41	498	143.078 37.960
3009	05:54:41	498	143.519 37.395
0559	05:54:44	501	143.104 38.955
0945	05:54:46	503	143.264 38.398
3002	05:54:47	504	143.077 37.701
0215	05:54:48	505	142.989 37.800
3010	05:54:48	505	143.288 37.420
0217	05:54:49	506	142.956 38.255
0209	05:54:50	507	142.801 38.639
0797	05:54:50	507	143.527 39.284
0584	05:54:51	508	143.105 37.485

[a]First 45 sec.

perturbation within first 15 seconds in the area 37.7-38.13°N (Figure 1b).

[15] Very similar image was captured by the arrivals of the CID' first peaks (Figure 1c and Table S1 from the auxiliary material). The first maximum was registered 469 sec after the earthquake at station 0214. Arrivals of CID within first 45 seconds imaged a region (37.39 - 39.28°N; 142.8 – 143.73°E). Observing that the perturbation further spreads away from this area, we conclude this rectangle to be the source of the CID. Knowing that CID can be only generated by coseismic vertical movements of the ground/sea floor, and that the maximum of acoustic energy release corresponds to a focal area, it seems reasonable to presume that first arrivals of TEC observations indicate the area of vertical uplift that occurred during the Tohoku earthquake. Figure 1a shows coseismic vertical displacements calculated by the model of *Okada* [1992] and using the coseismic slip distribution by the USGS (http://earthquake.usgs.gov). Indeed, comparison of our results with the models of coseismic crustal deformations shows that the obtained ionospheric image corresponds to the area of the maximum uplift (Figures 1a–1c).

[16] More detailed analysis of the first arrivals could therefore provide information on the propagation of seismic rupture during the earthquake. To obtain the dynamic characteristics of the CID, we calculated the propagation speed and direction of propagation of perturbations by use of method of GPS-arrays [*Afraimovich et al.*, 2001]. The horizontal projection of the phase velocity and the direction are estimated from the time delays between three GPS receivers considered as GPS-array. Our calculations showed that from the first arrival point (site 0214) the CID propagated first north-westward (318°, calculated clockwise from the azimuth) with a velocity ~3.0 km/s. From 15 to 45 seconds the CID simultaneously propagates westward (292°) with velocity 1.3 km/s and south-westward (196°) with the velocity 1.5 km/s. The CID afterwards propagates on the west and south-west at ~1.6 km/s. Apparently, the first arrivals show the rupture propagation and forming of the CID, whereas starting from 45 sec after the first arrival we observe propagation of ionospheric disturbances outward the source.

[17] It should be noted that the value 1.3-1.5 km/s is 30-40% higher than previously reported propagation velocities of CID in the near-field of the epicenter [e.g., *Afraimovich et al.*, 2001; *Heki and Ping*, 2005; *Astafyeva et al.*, 2009]. Apparently, after the Tohoku-oki earthquake we observe shock-acoustic waves propagating at supersonic speed. This fact is coherent with registration of the first arrival of perturbation 464 sec after the earthquake that is, generally speaking, too short time for a regular acoustic wave to reach the ionosphere.

4. Discussions and Conclusions

[18] The preliminary USGS NEIC finite fault slip models generated within first 7 hours of the earthquake time indicated that event ruptured a fault up to 300 km long, roughly centered on the earthquake hypocenter, and involved peak slips of 20 m or more [*Hayes*, 2011]. Updated model was released approximately 3 days after the quake and showed that peak slip of ~32 m was elongated in the north-east – southwestern direction and located ~70-90 km on the east from the epicenter. Kinematic fault slip models estimated the time of the rupture as ~100 seconds to cover region from the epicenter to 36.9 and to 38.9°N, with maximum vertical displacement up to 8 m [*Simons et al.*, 2011].

[19] Our analysis showed the possibility to obtain information on coseismic vertical displacements from ionospheric TEC. In the case of the great M9.0 Tohoku megathrust earthquake, the ionospheric images for the seismic fault slip manifested itself in the ionosphere 509 seconds after the quake. The area (37.39 - 39.28°N; 142.8 – 143.73°E) imaged by SIP within first 45 seconds after the first arrival of perturbation coincides with the area of the coseismic crustal vertical displacements. From this source-region the CID propagated simultaneously north-westward and south-westward first with velocity 3 km/s, showing the rupturing fault, and then with 1.3-1.5 km/s, showing propagation of CID. Unfortunately, the geometry of the GPS-sounding for PRN26 does not let observations of CID on the east from the original area.

[20] The TEC maximum values were registered from 469 sec after the earthquake. Simple calculations show that for 470–500 sec the "regular" acoustic waves would reach ~190-200 km of altitude. This might be too low for GPS-detection, as we consider that ionospheric perturbations are registered at the altitude of maximum of electron concentration. As was mentioned above, GPS-sounding and the integral character of TEC do not allow the exact altitudinal localization of the detected ionospheric perturbation. Here we assumed the altitude of the ionospheric sounding points h_{max} =250 km that is 30 km lower than the maximum of the ionosphere F2-layer as measured at Kokubunji ionospheric station in Japan (http://spidr.ngdc.nasa.gov). Such choice of h_{max} is related to the early arrivals of perturbation, that are along with large TEC amplitudes will likely be challenging for further modeling. Figure 3a illustrates the integrated electron content as a value of the

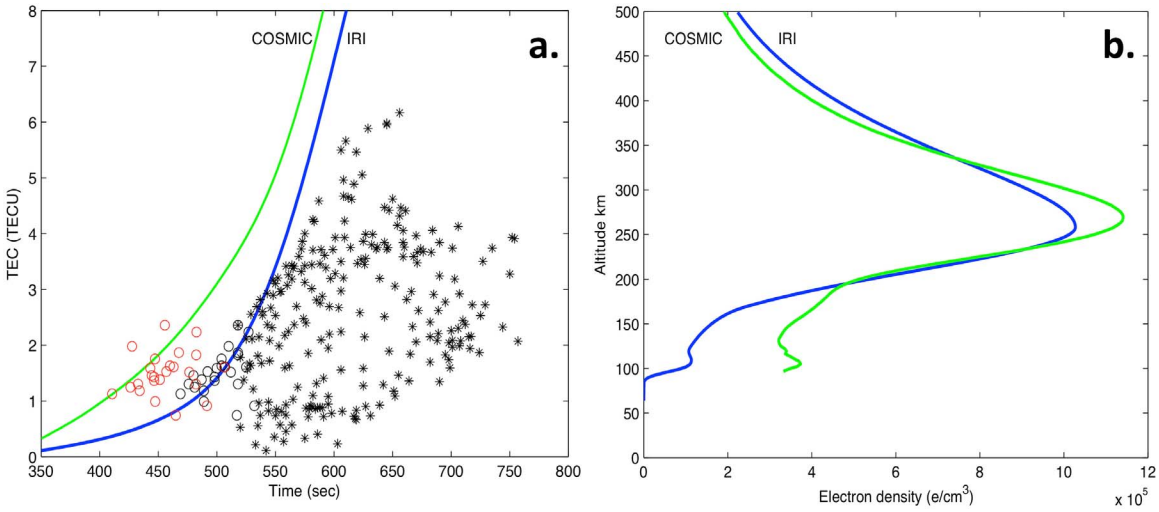

Figure 3. (a) Relation between TEC and the CID arrival times as obtained by modeling and observations. The curves indicate integrated electron density between the ground and a given altitude z as a function of the vertical propagation time from the ground to this altitude, calculated for the IRI-2007 results (blue curve) and for COSMIC-2 satellite measurements (green curve). The propagation time is calculated for acoustic waves propagating in the atmosphere modeled by the MSISE-00 [*Picone et al.*, 2002]. Black circles show amplitude of the GPS-observed first 24 arrivals (as in Table S1 from the auxiliary material) as function of arrival time, stars represent later arrivals. Red circles correspond to the "corrected" arrival times, i.e. without the time of rupture propagation. (b) Electron density profiles measured by COSMIC-2 satellites (green curve) and modeled by the IRI-2007 (blue curve).

vertical acoustic propagation time instead of altitude and the observed amplitude, and time of the first maximums of the ionospheric signals for all data points from PRN26. The travel time of acoustic waves is computed from MSISE-00 [*Picone et al.*, 2002], and the TEC - from IRI-07 [*Bilitza and Reinisch*, 2008]. It is seen that within first 45 sec the observations are close to the absolute limit of all the integrated electrons (as indicated by black circles). The first arrivals demonstrate not only very short travel time but also that the amplitudes of TEC observations are close to the maximum of TEC integrated below the corresponding altitude (Figure 3a). This would suggest that the propagating wave blows off and carries all the electrons available from the ground to the altitude of detection. The first arrivals are therefore very much different from those at larger distances (shown by stars), corresponding to travel times of 600 sec or more.

[21] It should be remembered that in the case of the Tohoku earthquake, the epicenter was located at ~100-120 km from the maximum fault slip, so that it took at least 46 seconds to rupture from the epicenter to the maximum slip. Therefore, the "real" time of upward propagation of waves from the uplift to the atmosphere/ionosphere is even less than 464 sec (these points are shown in Figure 3 as red circles) and, subsequently, the altitudes of registration of the regular acoustic waves could be even lower than 180 km. The latter is however much less probable, as follows from the altitudinal profiles of electron density (Figure 3b). At the same time, observations by COSMIC satellites around the earthquake's epicenter on 11 March 2011 show much larger number of electrons than modeled by IRI-2007 at 100–200 km of height (Figure 3a). This could partially explain the early arrivals along with large amplitude of the observed TEC perturbations, though some points are still very close to the "limits". We therefore suppose that we observed propagation of shock-acoustic waves that carry the majority of the available electron content, possibly with some supersonic regime at low altitudes. The calculated horizontal CID velocities of 1.3-1.5 km/s also go to show that we observe propagation of shock-acoustic waves. Their full understanding, however, will request non-linear shock waves modeling that is beyond the scope of the current work.

[22] Apart from these new challenges in the modeling of seismo-ionosphere coupling, our study demonstrates that the first CID arrivals provide an image of the seismic fault generated vertical displacement, its location and dimensions about 8 minutes after the quake. According to the Japan Meteorological Agency (http://www.jma.go.jp), on 11 March 2011 the first arrival of the tsunami maximum readings ranged from 06:12 UT to 06:21 UT, i.e. between 26 and 35 minutes after the earthquake had struck. The 17 minutes of remaining time open therefore the perspective to use real time GPS data for improving rapid determination of the maximum sea-level uplift and therefore better update of the near-field tsunami warning systems.

[23] **Acknowledgments.** E.A. and L.R. were supported by the French National Space Agency (CNES), with additional support from CNES and ONR for 1 Hz GPS data purchase. This work, in general, is supported by the French National Research Agency (ANR), project "To_EOS". We are grateful to Kosuke Heki (Hokkaido University, Japan), Kouji Matsuo (Hokkaido University, Japan), Sébastien Allgeyer (ENS-CEA, France), and François Beauducel (IPGP, France) for their help with modeling of coseismic vertical displacements. We thank Geospatial Information Authority of Japan for the data of the GPS Earth Observation Network System (GEONET). This is IPGP contribution 3237.

[24] The Editor thanks Kosuke Heki and an anonymous reviewer for their assistance in evaluating this paper.

References

Afraimovich, E. L., N. P. Perevalova, A. V. Plotnikov, and A. M. Uralov (2001), The shock-acoustic waves generated by the earthquakes, *Ann. Geophys.*, *19*(4), 395–409, doi:10.5194/angeo-19-395-2001.

Astafyeva, E. I., and E. L. Afraimovich (2006), Long-distance propagation of traveling ionospheric disturbances caused by the great Sumatra-Andaman earthquake on 26 December 2004, *Earth Planets Space*, *58*, 1025–1031.

Astafyeva, E., and K. Heki (2009), Dependence of waveform of near-field coseismic ionospheric disturbances on focal mechanisms, *Earth Planets Space*, *61*, 939–943.

Astafyeva, E., K. Heki, V. Kiryushkin, E. L. Afraimovich, and S. Shalimov (2009), Two-mode long-distance propagation of coseismic ionosphere disturbances, *J. Geophys. Res.*, *114*, A10307, doi:10.1029/2008JA013853.

Bilitza, D., and B. Reinisch (2008), International Reference Ionosphere 2007: Improvements and new parameters, *Adv. Space Res.*, *42*(4), 599–609, doi:10.1016/j.asr.2007.07.048.

Calais, E., and J. B. Minster (1995), GPS detection of ionospheric perturbations following the January 17, 1994, Northridge earthquake, *Geophys. Res. Lett.*, *22*, 1045–1048, doi:10.1029/95GL00168.

Hayes, G. P. (2011), Rapid source characterization of the 03-11-2011 Mw 9.0 Off the Pacific Coast of Tohoku Earthquake, *Earth Planets Space*, *63*, 529–534, doi:10.5047/eps.2011.05.012.

Heki, K., and J. Ping (2005), Directivity and apparent velocity of the coseismic ionospheric disturbances observed with a dense GPS array, *Earth Planet. Sci. Lett.*, *236*, 845–855, doi:10.1016/j.epsl.2005.06.010.

Heki, K., Y. Otsuka, N. Choosakul, N. Hemmakorn, T. Komolmis, and T. Maruyama (2006), Detection of ruptures of Andaman fault segments in the 2004 great Sumatra earthquake with coseismic ionospheric disturbances, *J. Geophys. Res.*, *111*, B09313, doi:10.1029/2005JB004202.

Kherani, E. A., P. Lognonné, N. Kamath, F. Crespon, and R. Garcia (2009), Response of the ionosphere to the seismic triggered acoustic waves: Electron density and electromagnetic fluctuations, *Geophys. J. Int.*, *176*, 1–13, doi:10.1111/j.1365-246X.2008.03818.x.

Klobuchar, J. A. (1986), Ionospheric time-delay algorithm for single frequency GPS users, *IEEE Trans. Aerosp. Electr. Syst.*, *23*(3), 325–331.

Liu, J.-Y., C.-H. Chen, C.-H. Lin, H.-F. Tsai, C.-H. Chen, and M. Kamogawa (2011), Ionospheric disturbances triggered by the 11 March 2011 *M*9.0 Tohoku earthquake, *J. Geophys. Res.*, *116*, A06319, doi:10.1029/2011JA016761.

Lognonné, P., J. Artru, R. Garcia, F. Crespon, V. Ducic, E. Jeansou, G. Occhipinti, J. Helbert, G. Moreaux, and P. Godet (2006), Ground-based GPS imaging of ionospheric postseismic signal, *Planet. Space Sci.*, *54*, 528–540, doi:10.1016/j.pss.2005.10.021.

Makela, J. J., et al. (2011), Imaging and modeling the ionospheric airglow response over Hawaii to the tsunami generated by the Tohoku Earthquake of 11 March 2011, *Geophys. Res. Lett.*, *38*, L00G02, doi:10.1029/2011GL047860.

Okada, Y. (1992), Internal deformation due to shear and tensile faults in a half-space, *Bull. Seismol. Soc. Am.*, *82*, 1018–1040.

Picone, J. M., A. E. Hedin, D. P. Drob, and A. C. Aikin (2002), NRLMSISE-00 empirical model of the atmosphere: Statistical comparisons and scientific issues, *J. Geophys. Res.*, *107*(A12), 1468, doi:10.1029/2002JA009430.

Rolland, L., P. Lognonne, and H. Munekane (2011a), Detection and modeling of Rayleigh wave induced patterns in the ionosphere, *J. Geophys. Res.*, *116*, A05320, doi:10.1029/2010JA016060.

Rolland, L., P. Lognonne, E. Astafyeva, A. Kherani, N. Kobayashi, M. Mann, and H. Munekane (2011b), The resonant response of the ionosphere imaged after the 2011 Tohoku-Oki earthquake, *Earth Planets Space*, *63*, 853–857, doi:10.5047/eps.2011.06.020.

Simons, M., et al. (2011), The 2011 magnitude 9.0 Tohoku-oki earthquake: Mosaicking the megathrust from seconds to centuries, *Science*, *332*(6036), 1421–1425, doi:10.1126/science.1206731.

E. Astafyeva, P. Lognonné, and L. Rolland, Institut de Physique du Globe de Paris, Paris Sorbonne Cité, Université Paris Diderot, UMR 7154, CNRS, 4 Ave. de Neptune, Saint Maur des Fossés F-94107, France. (astafyeva@ipgp.fr)